The Astrophysical Journal, 783:111 (7pp), 2014 March 10 doi:10.1088/0004-637X/783/2/111

EXPERIMENTAL STUDY ON BOUNCING BARRIERS IN PROTOPLANETARY DISKS

T. Kelling, G. Wurm, and M. Köster
Faculty of Physics, University Duisburg-Essen, Lotharstr. 1, D-47057 Duisburg, Germany; thorben.kelling@uni-due.de
Received 2013 September 27; accepted 2014 January 16; published 2014 February 21

ABSTRACT

For dust aggregates in protoplanetary disks, a transition between sticking and bouncing in individual collisions at mm to cm sizes has been observed in the past. This leads to the notion of a bouncing barrier for which growth gets stalled. Here, we present long-term laboratory experiments on the outcome of repeated aggregate collisions at the bouncing barrier. About 100 SiO_2 dust aggregates 1 mm in size were observed interacting with each other. Collisions occurred within a velocity range from below mm s^{-1} up to cm s^{-1}. Aggregates continuously interacted with each other over a period of 900 s. During this time, more than 10^5 collisions occurred. Nearly 2000 collisions were analyzed in detail. No temporal stable net growth of larger aggregates was observed even though sticking collision occurred. Larger ensembles of aggregates sticking together were formed but were disassembled again during further collisional evolution. The concept of a bouncing barrier supports the formation of planetesimals by seeded collisional growth, as well as by gravitational instability favoring a significant total mass being limited to certain size ranges. Within our parameter set, the experiments confirm that bouncing barriers are one possible and likely evolutionary limit of self-consistent particle growth.

Key words: planets and satellites: formation – protoplanetary disks

1. INTRODUCTION

There has been tremendous progress in recent years concerning the assembly of km-sized planetesimals as an early phase of planet formation. In a first step, dust grains couple well to the gas in protoplanetary disks and collide gently enough that sticking and growth of (initially fractal) dust aggregates is warranted (Chokshi et al. 1993; Dominik & Tielens 1997; Wurm & Blum 1998; Blum & Wurm 2000, 2008; Blum et al. 2000; Paszun & Dominik 2006; Wada et al. 2009; Birnstiel et al. 2012). In some cases, charging might prevent collisions, as suggested by Okuzumi (2009). In other cases, charges accelerate the process (Konopka et al. 2005). However, in the dense midplane, charging is unlikely to occur and growth of mm-sized aggregates is undisputed.

There is little doubt that very porous, fractal aggregates evolve initially. However, the energy eventually is enough to restructure particles. With micrometer silicate grains, this occurs at cm sizes, as experimentally shown by Blum and Wurm (2000) at low speed. While the aggregates that get compacted now are still initially highly porous, they are compacted by further collisions even at low speeds, far below 1 m s^{-1}. This has been shown by Weidling et al. (2009), who found in laboratory experiments that a filling factor of 0.36 results after a large number of collisions of an individual mm-sized dust aggregate. As detailed below, this matches the volume filling factor used in the experiments reported here. For this later stage, Zsom et al. (2010) proposed a bouncing barrier for this size range based on experimental results (Blum & Wurm 2008; Heißelmann et al. 2010). The basic physics behind the bouncing is that dust aggregates have been restructured by previous collisions and are more or less compact now. As collision velocities are still well below a m s^{-1} speed, no significant energy dissipation by further restructuring is possible. The collisions are essentially elastic and rebound is likely. Bouncing has been studied in experiments (Weidling et al. 2012) and numerical simulations, e.g., by Wada et al. (2011) or Seizinger & Kley (2013), and bouncing is also present in experiments with larger solid impactors at low velocities (Colwell 2003; Colwell et al. 2008). This paper is focused on this stage of pre-planetesimal evolution and we do not consider the initial collisions of very fluffy mm-dust aggregates of low filling factor as we explicitly perform experiments to probe the proposed bouncing barrier.

The behavior of water ice as solid beyond the snow line might be somewhat different but sticking and bouncing (and fragmentation) are also observed and simulated for ice particles (Supulver et al. 1995; Higa et al. 1998; Schäfer et al. 2007; Wada et al. 2009; Okuzumi et al. 2012). This might shift the bouncing barrier to larger sizes. Sublimation, condensation, and sintering are important processes here that might change the setting quite a bit though (Saito & Sirono 2011; Sirono 2011; Aumatell & Wurm 2011; Ros & Johansen 2013). We only consider refractory dust in our experiments reported here.

Seemingly an obstacle to planetesimal formation, the bouncing barrier for dust aggregates of a certain size (mm to cm) might be an important milestone for planetesimal formation. There are two possibilities on how to proceed from here on the way to planetesimals.

If the gas densities or the location in the disk is right, turbulence, stable eddies, or streaming instabilities might concentrate solids that then get bound gravitationally and support the formation of larger objects rather quickly (Johansen et al. 2007; Cuzzi et al. 2008; Chiang & Youdin 2010; Dittrich et al. 2013). These studies, so far, do not include collisional physics. If conditions are less favorable, larger initial particle sizes (i.e., decimeter) are needed in a significant amount but mm sizes might be sufficient in some cases. The rapid formation of planetesimals within a few orbital timescales would also decrease the problem (or even use it in a streaming instability) that solid particles drift inward. This radial drift, estimated to be as large as 1 AU in 100 yr, has been a Sword of Damocles for a long time (Weidenschilling 1977). The problem might also be solved by considering more complex or realistic disk models with pressure bumps or disk edges in different locations where particles would be concentrated (Barge & Sommeria 1995; Klahr & Henning 1997; Brauer et al. 2008; Pinilla et al. 2012; Ayliffe et al. 2012).

The second way to proceed from mm particles to planetesimals is still a model of collisional growth. This is also not without further assumptions to be detailed in future work, but Windmark et al. (2012a) showed that some seeds of larger size are enough to promote growth. This is based on the fact that collisions with larger objects get faster (tens of m s^{-1}) and accretion is now possible again, as seen in a series of experiments (Wurm et al. 2005; Teiser & Wurm 2009; Kothe et al. 2010; Teiser et al. 2011b). This requires some particles to jump over the bouncing barrier and act as seeds for further growth. Windmark et al. (2012b) proposed that slow collisions in a turbulent disk—unlikely as they might be—could provide a small number of seeds. This might go together with results from microgravity experiments that once a number of compact aggregates form a new aggregate this allows further growth over some velocity range (Weidling et al. 2012; Kothe et al. 2013). From a set of different laboratory experiments, Jankowski et al. (2012) found that sticking probabilities are enhanced if the aggregates are composed of grains 10 μm in size instead of smaller grains. These are on the upper end of reasonable grain sizes in disks but might—even if in small number—seed further growth.

Whatever the process to form planetesimals, eventually, the fact that the bouncing barrier is actually needed or at least very beneficial for the further evolution is important. If all particles can grow, the process would stall in a collisional model; especially at larger size, collisions between equal-size aggregates will destroy particles, even at low collision speeds. This has, for example, been seen in experiments on dust aggregate collisions from cm to dm by Beitz et al. (2011), Schräpler et al. (2012), and Deckers & Teiser (2013). When small particles below the bouncing barrier are present, a small number of large objects can grow on their account. If no bouncing (or fragmentation) barrier exists, too small particles might be present in the critical size range of Stokes number 1 needed in the gravitoturbulent or streaming-instability models.

Either way, bouncing of a significant part of, e.g., mm aggregates – although counterintuitive as it might be—is likely a key process to forming larger bodies.

So far, the bouncing barrier had only been studied in individual collisions. Small probabilities for sticking two mm-sized aggregates together exist and suggest that continuous growth might be possible (Weidling et al. 2012; Jankowski et al. 2012; Kothe et al. 2013). However, detachment in a further collision might also prevent further growth as the connection between two compact dust aggregates is very weak (Jankowski et al. 2012). In a somewhat different setting—in Saturn's rings—but putting an emphasis on weak connections, particle release is also discussed (Bodrova et al. 2012). Therefore, the study of individual collisions is not enough to answer if further growth is possible. In this paper, we study the long-term collisional evolution of a large number of mm-sized aggregates in a laboratory experiment. We show that the bouncing barrier is indeed a robust part of collisional evolution in protoplanetary disks.

2. EXPERIMENTS

It was only recently discovered that sub-mm to cm sized dust and ice aggregates as highly porous objects can be levitated in a temperature gradient field at low ambient pressure over a smooth surface (Kelling & Wurm 2009; Kelling et al. 2011; Aumatell & Wurm 2011; Jankowski et al. 2012). The lift is generated as the particles act like Knudsen compressors (see below). Kelling & Wurm (2009) and Jankowski et al. (2012) showed that large numbers of aggregates are easily levitated at the same time.

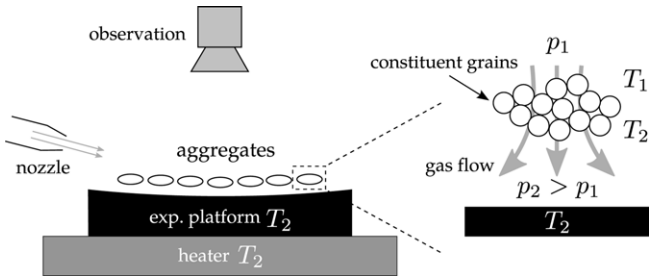

Figure 1. Experimental setup is placed within a vacuum chamber. ~100 flat, cylindrically shaped SiO_2 aggregates are placed on a slightly concave platform with a heater below. A camera observes the ensemble from above and a gas flow through a nozzle can be used to enhance the relative velocity between the aggregates. The aggregates are levitated as they become Knudsen compressors (see the text for details).

Table 1
Aggregate Details and Collision Events

Eq. radius $\bar{r}_{agg}$	(515 ± 40) μm	
Height h_{agg}	(200 ± 30) μm	
Mass m_{agg}	$(2.13 \pm 0.05) \times 10^{-7}$ kg	
Density ρ	2650 kg m^{-3}[a]	
Filling factor f	0.36 ± 0.01	
	Non-excited	Excited
Number of aggregates		
Total	110	111
High speed	Non-excited	Excited
Rec. time	8175 ms	8175 ms
Mean $\bar{v}_{col}$	4.0 mm s^{-1}	7.4 mm s^{-1}
Collisions	348	1515
Long term	Non-excited	Excited
Rec. time	900 s	900 s
Collisions	38.312[b]	166.789[b]

Notes.
[a] Constituent grains.
[b] Extrapolated from high-speed recording.

The composition can vary, e.g., aggregates from SiO_2, basalt, or graphite powder with a broad size distribution might be levitated. We used this experimental technique here to generate over 100 free-moving, mm-sized SiO_2 (quartz) aggregates. This material was used frequently in past experiments. The constituent grains are between 0.1 and 10 μm in size with 80% of the grains between 1 and 5μm (Sigma Aldrich; Table 1). The basic experimental setup is shown in Figure 1. The experimental setup is placed within a vacuum chamber. A heater is coupled to a slightly concave and black platform (radius 30 mm, center depth 0.8 mm) on which ~100 flat, cylindrical SiO_2 dust aggregates are placed. The aggregates used in the experiments are shown in Figure 2. The slightly concave shape of the experimental platform ensures that the levitating aggregates are gently forced to move toward the center of the platform, which prevents them from leaving the platform but forces them to interact with each other. A nozzle is installed some cm distance from the levitating aggregates to excite the aggregate assemble through an air flow. With this gas flow, the collisional velocity of the aggregates can be enhanced. A camera capturing images at 200 frames s^{-1} is used to study the details of the motion and the collisions of the aggregates (high-speed recording phase). For the long-term recording, a second camera takes an image of the set every 3 s over a total time period of 15 minutes (long-time recording

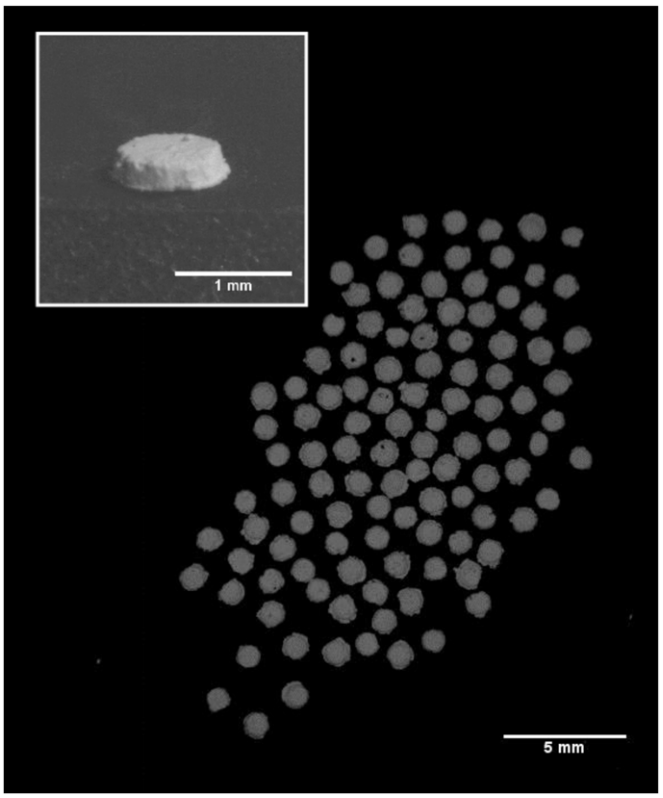

Figure 2. SiO_2 aggregate sample, as observed by the high-speed camera. The inset is a microscope image of one of the aggregates.

phase). The ambient gas pressure is set to $p = 15 \pm 1$ mbar and the heater temperature is set to $T_2 \simeq 800$ K.

The mechanism behind the levitation of the aggregates is temperature-driven gas flow (thermal creep) through the dust aggregates and a resulting pressure build-up below (Knudsen compressor). Knudsen (1909) showed that a gas flow is generated by temperature gradients, which can establish an overpressure. In his experiments, Knudsen (1909) connected two gas reservoirs at different temperatures T_1 and $T_2 > T_1$ by a tube with diameter d_t (small compared with the mean free path λ of the gas molecules; $d_t \ll \lambda$). In equilibrium, the pressure p_1 and p_2 in the two chambers are related by

$$\frac{p_2}{p_1} = \sqrt{\frac{T_2}{T_1}}. \quad (1)$$

With a cascade of several connected chambers, Knudsen (1909) reached a compression ratio of $p_2/p_1 \simeq 10$ between the first and the last chamber. Muntz et al. (2002) showed that the overpressure $\Delta p = |p_1 - p_2|$ at intermediate Knudsen numbers Kn in the warmer chamber is

$$\Delta p = p_{\rm avg} \frac{\Delta T}{T_{\rm avg}} \frac{Q_T}{Q_P}. \quad (2)$$

It is $p_{\rm avg} = (p_1 + p_2)/2$ the average pressure, $\Delta T = |T_1 - T_2|$ the temperature difference between the two gas reservoirs, $T_{\rm avg} = (T_1 + T_2)/2$ the average temperature, and Q_T/Q_P the ratio of the coefficients of the temperature-induced gas flow (Q_T) and the back flow of the gas (Q_P). Values for Q_T/Q_P are given by Muntz et al. (2002). The Knudsen number $\mathrm{Kn} = \lambda/d$ is defined as the ratio of the mean free path of the gas molecules to a relevant geometric length d.

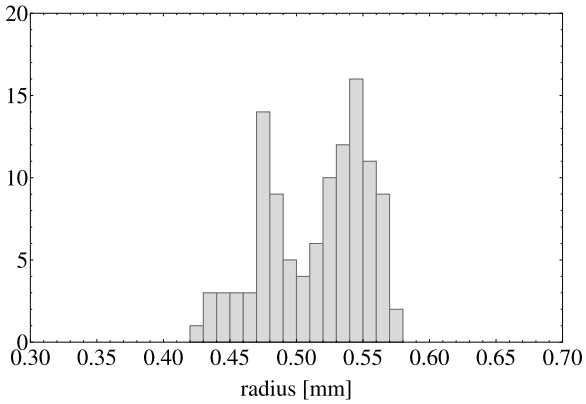

Figure 3. Size distribution of the aggregates. The radii r are two-dimensional equivalent radii calculated from the imaged cross section A of an aggregate ($r = \sqrt{A/\pi}$).

Dust aggregates are not solid bodies but have pores at approximately the same size as their constituent grains (Jankowski et al. 2012). These pores form channels that connect the gas volume above the aggregate with the gas volume below the aggregate. Hence, an aggregate can be interpreted as a collection of microchannels. The heater heats the bottom of the aggregates. The heat is transported by thermal conductivity through the aggregate toward the top where thermal radiation cools the aggregate. A temperature difference between the bottom and the top is established and gas flows through the aggregate (thermal creep). Depending on the thermal conductivity $\kappa_{\rm agg}$ and the thickness (height h) of the aggregate, a more or less prominent temperature difference ΔT is established between the inlet of the microchannels (top side, $T_1 < T_2$) and the outlet (bottom side, $T_2 > T_1$). The temperatures T_1 and T_2 are related by (neglecting the ambient temperature)

$$\sigma T_1^4 = \frac{\kappa_{\rm agg}}{h}(T_2 - T_1). \quad (3)$$

According to Equation (2), an overpressure is created below the aggregate. If the overpressure is sufficient, the aggregates are levitated. While levitating, the gas that is compressed by thermal creep through the aggregates escapes through the open sides below the aggregates (see also Figure 1). As we use dust with a similar grain size distribution, similar ambient gas pressure, and similar temperatures as Kelling & Wurm (2009) and Jankowski et al. (2012), we have the following values: the thermal conductivity of the aggregates ($\kappa_{\rm agg} \simeq 0.1$ W (m K)$^{-1}$), the temperature difference over the aggregates ($\Delta T \simeq 20$ K), and the resulting overpressure below the aggregates $\Delta p \simeq 5$ Pa. The ratio of the force lifting the aggregate induced by the overpressure $F_{\Delta p}$ to the gravitational force F_G is then $F_{\Delta p}/F_G \simeq 5$.

To allow contact-free levitation, the aggregates have to have a smooth bottom side. Also, to avoid any ambiguity due to different size, mass, or shape, we did not choose particle aggregates randomly but prepared them in a specific manner. The dust was filled into molds within a thin steel plate, manually compressed, and any excess dust was scraped off along the top of the plate. The dust was then knocked out of their molds, resulting in the given flat cylindrical aggregates with smooth top and bottom sides. The mean of the size distribution of the aggregates radii is 515 μm (Figure 3). We carried out collision experiments with and without excitation by minor amounts of air through a nozzle. The velocity distributions of the aggregates is shown in Figure 4.

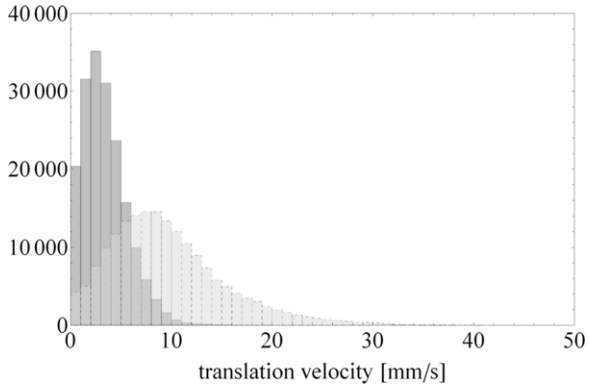

Figure 4. Translation velocity distribution of the aggregates with (light gray, dashed) and without excitation (dark gray, solid). The translation velocity is determined from frame to frame in the high-speed recording phase.

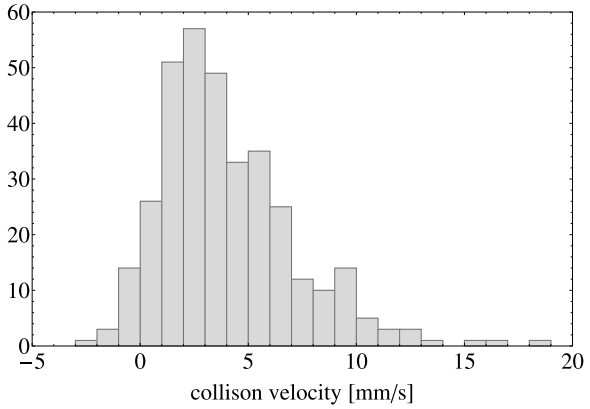

Figure 5. Collision velocity distribution without excitation. A negative velocity means that the two aggregates move away from each other but collide due to rotation.

3. COLLISIONS

Table 1 lists the details of the aggregates and collision events gained through the high-speed recording phase and the extrapolated events for the long-term recording. The filling factor of $f = 0.36$ is appropriate for compact dust aggregates (Weidling et al. 2009; Zsom et al. 2010; Teiser et al. 2011a; Meisner et al. 2012). We note, again, that our experiments do not model the collisions of the first mm-sized aggregates that have much lower filling factors. The experiments reported here model a somewhat later phase when mm-sized dust aggregates are already compacted by collisions. The average collision velocity $\bar{v}_{\rm col}$ is shown in Table 1 and the distributions of the collision velocities with and without excitation are shown in Figures 5 and 6. A negative velocity means that the two aggregates move away from each other slowly while rotating and colliding with uneven parts of their rim.

Collisions were clearly visible in the high-speed recording phase. In addition, the aggregates influence each other's trajectories by non-contact interactions. This might be interpreted as an effect of the gas outflow below the aggregates, whose influence we estimate below. As there is no physical contact between the aggregates during these interactions, they are not counted as collision events.

To determine the collision details, we tracked the position of all aggregates in every frame taken during the high-speed recording phase. To automatically track the aggregates, the individual grayscale images are binarized: background and

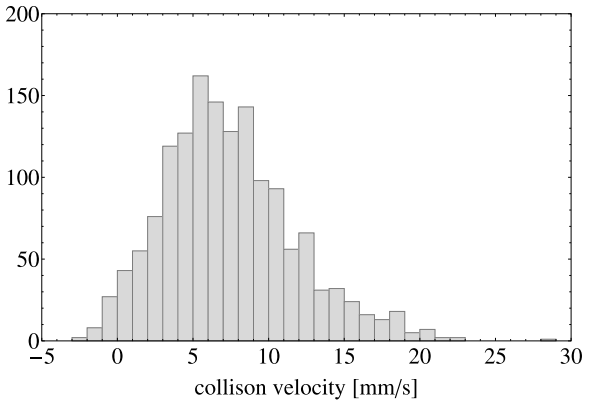

Figure 6. Collision velocity distribution with excitation. A negative velocity means that the two aggregates move away from each other but collide due to rotation.

aggregate pixel are separated by their gray value. The experimental platform is black while the aggregates reflect some of the light and appear brighter in the grayscale images. To ensure best results, we choose Otsu's algorithm (Otsu 1979) for the binarization. The choice of the binarization threshold (i.e., the gray value to separate background and aggregate) has an effect on the total collision number but almost no effect on the probabilities of the collisional outcomes (e.g., bouncing and sticking). Otsu's algorithm gives a relatively conservative number of collisions compared with other binarization algorithms and hence the total number of collisions in the experiments is rather underestimated as opposed to overestimated.

The time step between the individual images is 5 ms. An interaction between two aggregates is defined as a collision if the aggregates touch in at least one frame of the binarized image sequence. The boundary between sticking and bouncing is determined by two different timescales. One is the pure interaction time of colliding aggregates, which is the time two interacting aggregates need for a rebound; we estimate this time as follows: the minimum contact time for a bouncing collision can be estimated by elastic compression and relaxation of an aggregate by the other aggregate. With the modulus of elasticity E, the compression is defined as

$$\frac{F}{A} = -E\frac{(\Delta d)}{d}, \tag{4}$$

where F is the repelling force, A is the contact area, and d and Δd are the diameter and change in diameter of the aggregate, respectively. The force on the impinging aggregate is

$$F = ma = m\frac{d^2(\Delta d)}{dt^2}, \tag{5}$$

where m is the reduced mass. Combining Equations (4) and (5) results in

$$\frac{d^2(\Delta d)}{dt^2} = -\frac{EA}{md}(\Delta d), \tag{6}$$

which is a harmonic oscillator. Assuming $(\Delta d) = B\sin\omega t$ gives

$$\frac{d^2(\Delta d)}{dt^2} = -B\omega^2\sin\omega t. \tag{7}$$

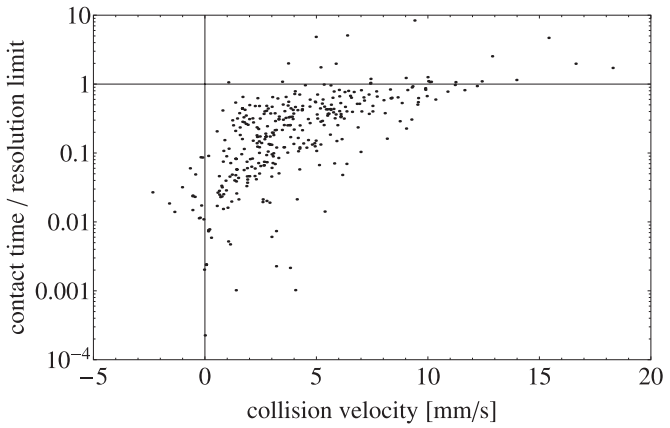

Figure 7. Ratio of the contact time of aggregates to the resolution time over the collision velocity for the non-excited case. For values below 1, no statement can be made if the event was sticking or bouncing. Values larger than 1 indicate sticking.

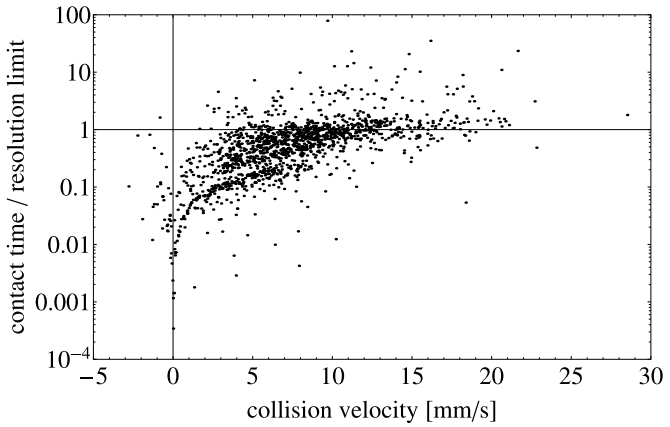

Figure 8. Ratio of the contact time of joined aggregates to the resolution time over the collision velocity for the excited case. For values below 1, no statement can be made if the event was sticking or bouncing.

With Equation (6) and the duration of a bouncing event $t_{\rm bounce}$, which is half a period or $\omega t_{\rm bounce} = \pi$, it is

$$t_{\rm bounce} = \pi \left(\frac{EA}{md} \right)^{-1/2}. \quad (8)$$

With $E \simeq 5 \times 10^6$ Pa (Meisner et al. 2012), $A = 10^{-8}$ m^2, $m \simeq 10^{-7}$ kg, and $d \simeq 1$ mm, the estimated bouncing time is $t_{\rm bounce} \simeq 0.1$ ms.

An aspect important to deciding whether a collision leads to sticking is the timescale set by the spatial resolution of the observation, which is $s = 46\,\mu$m. The resolution time is therefore determined by the time the aggregates need to traverse a length $4s$ ($2s$ for approaching and $2s$ for moving apart again, in the worst case). If two particles move away from each other again, the difference in the relative velocities before (index b) and after (index a) the interaction $C_I = v_a/v_b$ has to be considered. Within a time period of $t_{\rm resolve} = 2s/v_{\rm col} + 2s/(C_I v_{\rm col})$, two particles are observed to be in contact, even for a perfect bouncing event. In Figures 7 and 8, we show for all interaction events the ratio of the contact time (aggregates being visually in contact in the binarized images) to the individually calculated resolution time.

A value above 1 means that two aggregates are observed to be in contact longer then a potential bouncing event would last. For values below 1, no statement can be made if the interaction was a bouncing or a sticking event. In general, due to the resolution limit and the short timescales between successive collisions, the experiments do not allow one to classify a collision as bouncing. Values larger than 1 are a strong indication that the interaction was a sticking event. It has to be noted, however, that the reproach velocities are not rebound velocities. Therefore, we cannot rule out that, for example, two particles bounce off each other with a low coefficient of restitution and are observed to be one aggregate for a longer time and reproach fast after a second collision occurred. The resolution time calculated above is therefore a lower limit. Strictly speaking, the experiment does not allow one to quantify this delineation further. To judge this, well-separated collisions observable undisturbed for a sufficiently long time are needed. The larger the ratio between observed lifetime and resolution time, the less likely it is that the collision is bouncing.

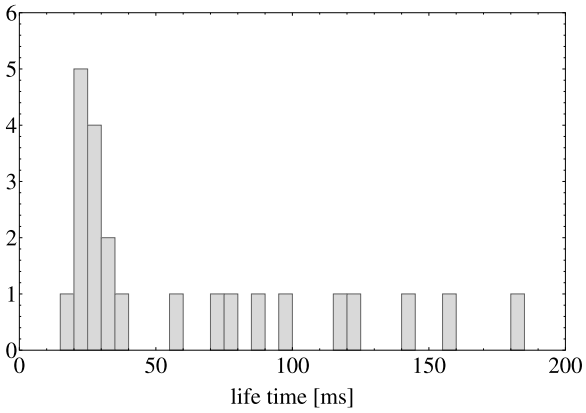

Figure 9. Distribution of the lifetimes of grown aggregates (high-speed recording phase, no excitation).

For the non-excited case, 93.3% of the collisions have ratios of the contact times to resolution times below 1; 6.7% are above 1 and 1.4% are above 2. The maximum ratio is 8. For the excited case, 76.4% are below 1, 23.6% are above 1, and 5.8% are above 2. The maximum ratio here is 79.

Beyond giving exact numbers for individual collisions, which is not the focus of this paper, there are sticking collisions (i.e., the ratios of contact times to resolution limit above 2). Proof of sticking collisions is aggregates that are not only in contact but also show bound rotation.

We classify the collisions with a ratio above 1 as aggregates stuck together. The observed distribution of the lifetimes of these grown aggregates are shown in Figures 9 and 10.

The analysis so far has concentrated on individual collisions. To estimate the temporal evolution of the aggregate ensemble, we observed the particle ensemble for 15 minutes, taking one image every 3 s. In case that growth is efficient, the number of aggregates should decrease from 110 to smaller values. Figure 11 shows the total number of aggregates during the high-speed recording phase and Figure 12 shows the total number of aggregates over the whole recording period of 15 minutes.

As our experimental platform is slightly concave and as there are non-contact forces between approaching aggregates (Knudsen compressor gas outflow below the aggregates), we estimate the strength of these effects. The force occurring during a pure rebound is given by Equation 4 and results in $F_{\rm reb.1} = 9 \times 10^{-6}$ N for the non-excited case and $F_{\rm reb.2} = 2 \times 10^{-5}$ N for the excited case. The slightly concave platform has a radius of 30 mm and is 0.8 mm deep at its maximum

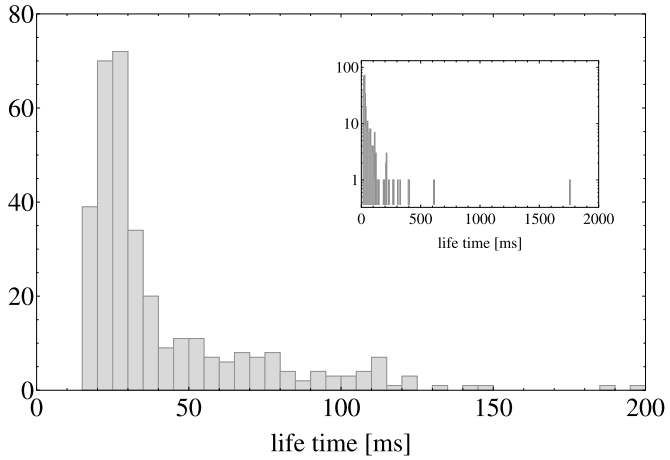

Figure 10. Lifetimes of aggregates. Same as Figure 9 but for the excited system. The inset shows the complete data, including the few extreme lifetimes.

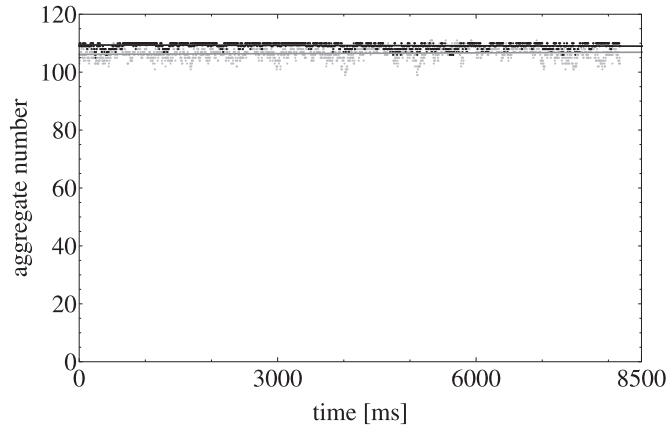

Figure 11. Total number of aggregates during the high-speed recording phase (dark gray: no excitation; light gray: with excitation). The solid lines are linear fits to the data.

(the center of the platform). The residual gravitational force acting on the aggregates pulls them together. In the worst case, this force is $F_{\mathrm{res}.G} = 4 \times 10^{-9}$ N. The deceleration of two approaching aggregates determines the non-contact pushing force (gas outflow because of the Knudsen compressor effect), which takes the value of $F_{\mathrm{Kn}} \simeq 10^{-11}$ N. We observe in our experiments that most grown aggregates break apart again without having made contact with other aggregates (95.7% in the non-excited case and 81.5% in the excited case). Hence, the non-contact forces (streaming gas, laboratory gravity), which are orders of magnitudes weaker than the forces occurring during a real collision event, are strong enough to break grown aggregates. In other words, if these weak non-contact forces are strong enough to break aggregates apart, any real collision would break grown aggregates for certain.

The majority of the individual collisions show a ratio of the contact time to the resolution limit well below 1 and hence no quantitative number can be given as to what fraction of the interactions were sticking or bouncing events. However, the exact number is of minor importance here. We do see a significant number of clear sticking events in individual interactions. Nevertheless, all grown aggregates break apart again. During the timescale of the experimental procedure, no stable net growth is observed. Expressed differently, after a time period of 15 minutes with more than 10^5 collisions or more than 1000 collisions per aggregate, no net growth is visible.

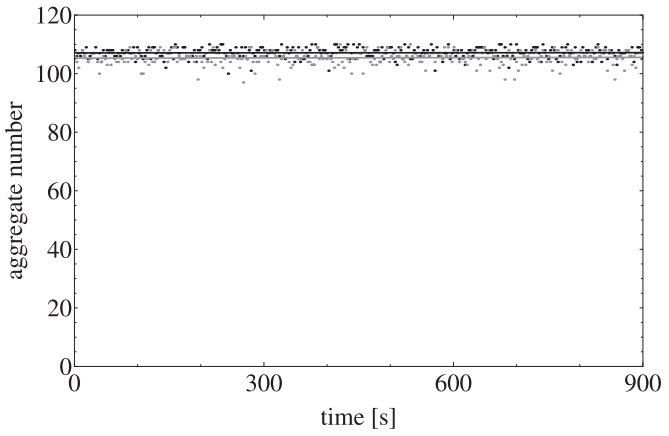

Figure 12. Total number of aggregates during the long time recording phase (dark gray: no excitation; light gray: with excitation). The solid lines are linear fits to the data.

4. APPLICATION TO PROTOPLANETARY DISKS

All of the aggregates in the experiment are moving freely. We do not have any evidence of contact with the surface of the heater. There are additional forces (streaming gas, laboratory gravity) acting on the aggregates in the laboratory that are not present in a protoplanetary disk. However, these forces are orders of magnitudes weaker than the force applied on an aggregate during an actual collision. If these forces are sufficient to break aggregates again, any real collision would break an aggregate as well (see the discussion at the end of Section 3). Therefore, we argue that the experiment is well suited to simulate collisions in protoplanetary disks. Also, as the collision velocity distributions do not depend on time, they simulate very well the analog situation of the disk, where collision velocities stay the same as the particles have enough time to couple to the gas in between two collisions. It is striking that we do not observe the stable growth of larger particles, although sticking in individual collisions is observed. Even after 1000 collisions, the individual aggregates are still individual aggregates. This is a perfect illustration of a bouncing barrier, as proposed by Zsom et al. (2010), and as found to be beneficial for further evolution by Windmark et al. (2012a).

On average, each particle collides 1500 times with other particles but does not grow (excited case). Compared with protoplanetary disks, this would simulate a timespan of 1×10^6 yr at 1 AU in a minimum-mass solar nebula, estimated as follows.

The gas density at 1 AU is about 10^{-6} kg m^{-3} (Hayashi et al. 1985). Assuming a dust-to-gas ratio of 1/100, the dust density is about 10^{-8} kg m^{-3}. If all mass is in mm-sized particles (volume 10^{-9} m^3) with a density of 1000 kg m^{-3} (low-density aggregates), one particle has a mass of 10^{-6} kg. This equals a particle number density of $n = 10^{-8}/10^{-6}$ m^{-3} or 10^{-2} m^{-3}. The timescale for a collision is $\tau = 1/(nv\sigma)$, with σ being the particle cross section (4×10^{-6} m^2) and $v = 10^{-3}$ m s^{-1}. This yields $\tau \simeq 3 \times 10^{10}$ s or approximately 1000 yr. Hence, 1500 collisions translate to about 1×10^6 yr in the disk (for a specific location, density, and velocity). Therefore, the bouncing barrier is very persistent, even if further collisions in the experiments eventually lead to the formation of larger aggregates. The latter is not expected, however. As there is no sign of growth in the experiments, the bouncing barrier can be considered to be very robust for the total duration of the disk lifetime.

The experiment only considered mm-sized aggregates of one composition and grain size, one filling factor of 36%, and a specific velocity distribution. This might be different in protoplanetary disks. At what particle size the barrier is actually located in a disk, depending on the radial distance to the star, is subject to future work.

5. CONCLUSIONS

Millimeter-sized dust aggregates are observed in protoplanetary disks (Rodmann et al. 2005). The accepted picture is that they grow by sticking collisions (Blum & Wurm 2008). The naive picture of a continuous particle growth by hit-and-stick beyond the size of mm or cm is certainly missing key points. Often discussed is the fragmentation barrier at sizes of meters. This means that particles that encounter large m-sized bodies do so with high speeds of 50 to 60 m s^{-1} and they might lose their integrity and not just stick to the m-sized body. More recently, Zsom et al. (2010) explicitly introduced the term "bouncing barrier" for compacted mm-sized particles. Here, the idea is that collisions of mm-sized dust aggregates with each other only leads to bouncing. While this process does not undo earlier growth, it does prevent further growth if no sticking occurs.

However, both processes—bouncing at small size and fragmentation at large size—might be beneficial for growth. Laboratory experiments by Wurm et al. (2005), Teiser & Wurm (2009), and Meisner et al. (2013) show that fragmentation at collision velocities up to 60 m s^{-1} do not necessarily destroy a large target body. While large parts of the projectile can be destroyed, this dissipation of kinetic energy still allows a fraction of several tens of percent of the projectile dust to stick to a larger target. Windmark et al. (2012a) showed that growth of larger seeds is possible if a bouncing barrier prevents all particles from growing at the same time. Collisional growth beyond the barriers is therefore possible if seeds are provided but the bouncing barrier in general is very important in that context.

In this paper, we studied the long-term collisional behavior of a set of about 100 equal dust aggregates about 1 mm in size at mm s^{-1} collision velocities. Individual collisions show some sticking efficiency but a dimer of two aggregates cannot just be regarded as a new particle with a different size, since the newly formed connection is rather weak compared with the internal structure of each of the two individual aggregates. Jankowski et al. (2012) already showed that detachment in a further collision produces the original aggregates, eventually, even though Jankowski et al. (2012) and Weidling et al. (2012) also find further attachments. So far, these were only individual collisions, however. Here, we study a total of over 10^5 collisions for 100 particles or 1000 collisions per mm-sized aggregate. We find sticking and detachment but no large aggregate that survived for long. In the end, no net growth was found. This is a perfect demonstration of a bouncing barrier, although in our experiments it might be better called a detachment barrier.

The parameters of the dust—μm grain size, mm aggregate size, mm s^{-1} collision velocities—are close to the values expected in protoplanetary disks. Applied to a disk, our simulation experiment would suggest that—without a seed—no further growth would be possible over the disk's lifetime in the terrestrial planet-forming region. If seeded growth or gravitational instabilities (Chiang & Youdin 2010) feeding on the mm- or cm-sized particles kicks in to form planetesimals remains to be seen. However, a bouncing (or detachment) barrier at mm to cm sizes is very likely an important milestone in planetesimal formation.

We acknowledge funding by the DFG as part of the research group FOR 759 and the project Ke 1897/1-1. We thank the anonymous reviewer for the comments.

REFERENCES

Aumatell, G., & Wurm, G. 2011, MNRAS, 418, L1
Ayliffe, B. A., Laibe, G., Price, D. J., & Bate, M. R. 2012, MNRAS, 423, 1450
Barge, P., & Sommeria, J. 1995, A&A, 295, L1
Beitz, E., Güttler, C., Blum, J., et al. 2011, ApJ, 736, 34
Birnstiel, T., Klahr, H., & Ercolano, B. 2012, A&A, 539, A148
Blum, G., & Wurm, G. 2000, Icar, 143, 138
Blum, G., & Wurm, G. 2008, ARA&A, 46, 21
Blum, J., Wurm, G., Kempf, S., et al. 2000, PhRvL, 85, 2426
Bodrova, A., Schmidt, J., Spahn, F., & Brilliantov, N. 2012, Icar, 218, 60
Brauer, F., Henning, T., & Dullemond, C. P. 2008, A&A, 487, L1
Chiang, E., Youdin, A. N., & Wurm, G. 2010, AREPS, 38, 493
Chokshi, A., Tielens, A. G. G. M., & Hollenbach, D. 1993, ApJ, 407, 806
Colwell, J., Sture, S., Cintala, M., et al. 2008, Icar, 195, 908
Colwell, J. E. 2003, Icar, 164, 188
Cuzzi, J. N., Hogan, R. C., & Shariff, K. 2008, ApJ, 687, 1432
Deckers, J., & Teiser, J. 2013, ApJ, 769, 151
Dittrich, K., Klahr, H., & Johansen, A. 2013, ApJ, 763, 117
Dominik, C., & Tielens, A. G. G. M. 1997, ApJ, 480, 647
Hayashi, C., Nakazawa, K., & Nakagawa, Y. 1985, Protostars and Planets II (Tucson, AZ: Univ. Arizona Press), 1100
Heißelmann, D., Blum, J., Fraser, H. J., & Wolling, K. 2010, Icar, 206, 424
Higa, M., Arakawa, M., & Maeno, N. 1998, Icar, 133, 310
Jankowski, T., Wurm, G., Kelling, T., et al. 2012, A&A, 542, 80
Johansen, A., Oishi, J. S., Mac Low, M. M., et al. 2007, Natur, 448, 1022
Kelling, T., & Wurm, G. 2009, PhRvL, 103, 215502
Kelling, T., Wurm, G., & Dürmann, C. 2011, RScI, 82, 115105
Klahr, H. H., & Henning, T. 1997, Icar, 128, 213
Knudsen, M. 1909, AnPhy, 336, 633
Konopka, U., Mokler, F., Ivlev, A. V., et al. 2005, NJPh, 7, 227
Kothe, S., Blum, J., Weidling, R., & Güttler, C. 2013, Icar, 225, 75
Kothe, S., Güttler, C., & Blum, J. 2010, ApJ, 725, 1242
Meisner, T., Wurm, G., & Teiser, J. 2012, A&A, 544, A138
Meisner, T., Wurm, G., Teiser, J., & Schywek, M. 2013, A&A, 559, 123
Muntz, E. P., Sone, Y., Aoki, K., Vargo, S., & Young, M. 2002, JVST, A, 20, 214
Okuzumi, S. 2009, ApJ, 698, 1122
Okuzumi, S., Tanaka, H., Kobayashi, H., & Wada, K. 2012, ApJ, 752, 106
Otsu, N. 1979, ITSMC, 9, 62
Paszun, D., & Dominik, C. 2006, Icar, 182, 274
Pinilla, P., Birnstiel, T., Ricci, L., et al. 2012, A&A, 538, A114
Rodmann, J., Henning, T., Chandler, C. J., Mundy, L. G., & Wilner, D. J. 2005, A&A., 446, 211
Ros, K., & Johansen, A. 2013, A&A, 552, A137
Saito, E., & Sirono, S. I. 2011, ApJ, 728, 20
Schäfer, C., Speith, R., & Kley, W. 2007, A&A, 470, 733
Schräpler, R., Blum, J., Seizinger, A., Kley, W., & Wilner, D. J. 2012, ApJ, 758, 35
Seizinger, A., & Kley, W. 2013, A&A, 551, A65
Sirono, A. 2011, ApJ, 735, 131
Supulver, K. D., Bridges, F. G., & Lin, D. N. C. 1995, Icar, 113, 188
Teiser, J., Engelhardt, I., & Wurm, G. 2011a, ApJ, 741, 5
Teiser, J., Küpper, M., & Wurm, G. 2011b, Icar, 215, 596
Teiser, J., & Wurm, G. 2009, MNRAS, 393, 1584
Wada, K., Tanaka, H., Suyama, T., Kimura, H., & Yamamoto, T. 2009, ApJ, 702, 1490
Wada, K., Tanaka, H., Suyama, T., Kimura, H., & Yamamoto, T. 2011, ApJ, 737, 36
Weidenschilling, S. J. 1977, MNRAS, 180, 57
Weidling, R., Güttler, C., & Blum, J. 2012, Icar, 218, 688
Weidling, R., Güttler, C., Blum, J., & Brauer, F. 2009, ApJ, 696, 2036
Windmark, F., Birnstiel, T., Güttler, C., et al. 2012a, A&A, 540, A73
Windmark, F., Birnstiel, T., Ormel, C. W., & Dullemond, C. P. 2012b, A&A, 544, L16
Wurm, G., & Blum, J. 1998, Icar, 132, 125
Wurm, G., Paraskov, G., & Krauss, O. 2005, Icar, 178, 253
Zsom, A., Ormel, C. W., Güttler, C., Blum, J., & Dullemond, C. P. 2010, A&A, 513, 56